2016 IEEE/RSJ International Conference on Intelligent Robots and Systems (IROS)
Daejeon Convention Center
October 9-14, 2016, Daejeon, Korea

# Feedback-Controlled Self-Folding of Autonomous Robot Collectives

Martin E. W. Nisser[1], Samuel M. Felton[1], Michael T. Tolley[2], Michael Rubenstein[3] and Robert J. Wood[1]

*Abstract*— **Self-folding provides an efficient way of creating complex 3D geometries from 2D composites. However, the precision of self-folding structures is often limited by the use of open-loop folding mechanisms. In this paper we demonstrate feedback-controlled self-folding using a shape memory polymer and optical sensors to accurately control folding angles. We present a method of quickly and inexpensively fabricating large collectives of self-folding autonomous robots that can be transported in flat configurations prior to autonomous deployment at target destinations. To demonstrate this, we build a collective of robots that is manufactured in one continuous laminar composite. Individual robots in the collective detach from one other, self-fold into pre-programmed configurations and navigate by phototaxis. This method could be applied to a broad range of applications where logistics necessitate compact transport and where external manipulation is difficult or expensive, such as in space applications or delivering search-and-rescue robots in cluttered environments.**

## I. INTRODUCTION

Folding is an effective means to fabricate 3D geometries quickly and inexpensively [1]. Tessellating and repeating patterns can be utilized to form metamaterials [2] with improved structural properties, or to package large structures into small volumes such as the origami-based Miura fold used to package solar panels flown on the Japanese satellite Space Flyer Unit [3]. Advances in computational origami have proven that from a single rectangular sheet, it is possible to create any connected polygonal region [4]. More recently, the freely available software Origamizer has provided a practical application of this idea by generating crease patterns for folding rectangular sheets into arbitrary polyhedrons without any cuts [5].

Folding is increasingly used within engineering as well [6]. Folded designs can be scaled effectively [7] and used to automate remote self-assembly. Furthermore, planar structures are compatible with a wide range of manufacturing techniques, and so prior to folding, the integration of system components such as batteries and integrated circuits can be automated using the same pick-and-place tools used to populate printed circuit boards [8].

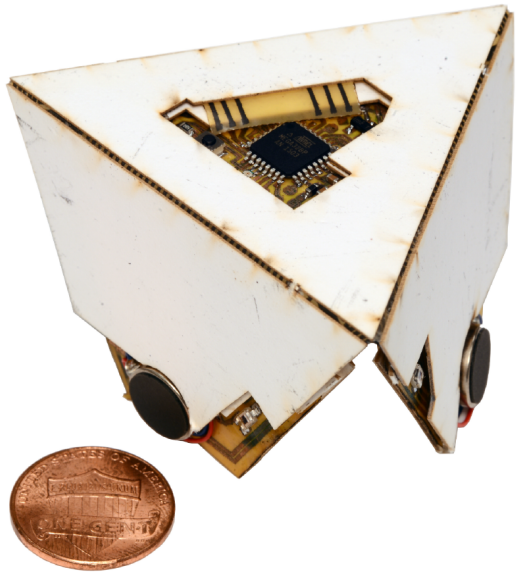

Fig. 1: A self-folded robot capable of autonomous navigation via phototaxis, manufactured in a laminar sheet as part of a self-assembling robot collective.

Self-folding has previously been enabled using shape memory alloy (SMA) [9] [10] [11], pneumatic actuators [12], various polymer films [13] and shape memory polymers (SMP) [14] [15]. SMPs are materials that undergo a one-way shape change when exposed to temperatures greater than their glass transition temperature ($T_g$). SMP actuators offer a pragmatic solution to structural folding as they will retain their folded shape without further stimulus, and can be cut with low-cost $CO_2$ lasers, allowing rapid fabrication of custom actuators. Their thermal activation can be targeted to provide local activation by either embedding resistive elements [16] or by exposure to infrared light [17], or actuation can be globally triggered over the entire structure by uniform heating in an oven [18] [19]. In particular, Shape Memory Composites (SMC) have been used to self-fold robots, fabricated by bonding together layers of different materials that include structural layers, embedded electronics, SMPs and flexure hinges. This process has been used in the development of several self-assembled structures including a robot inch-worm [16], a quadrupedal crawler [8] and structures with integrated electrical and mechanical sensors [20]. One drawback of this technique is precision: these robots exhibited fold angles up to 120° that were controlled

*The authors gratefully acknowledge support from the National Science Foundation (award numbers CCF-1138967 and EFRI-1240383) and the Wyss Institute for Biologically Inspired Engineering. Any opinions, findings and conclusions or recommendations expressed in this material are those of the authors and do not necessarily reflect those of the National Science Foundation.

[1]M. E. W. Nisser, S. M. Felton and R. J. Wood are with the Harvard John A. Paulson School of Engineering and Applied Sciences and the Wyss Institute for Biologically Inspired Engineering, Harvard University, Cambridge, MA 02138 martin.nisser@wyss.harvard.edu

[2]M. T. Tolley is with the Department of Mechanical and Aerospace Engineering, University of California, San Diego, La Jolla, CA 92093-0411 tolley@ucsd.edu

[3] M. Rubenstein is with the Department of Electrical Engineering and Computer Science, Northwestern University, Evanston, IL 60208 rubenstein@northwestern.edu

open-loop by varying the gap widths at the hinge. This method resulted in a standard deviation of $5^\circ$ for fold angles less than $100^\circ$ and $8^\circ$ when the fold angle was greater than $100^\circ$ [8]. The magnitude of these errors was particularly hindering to the creation of more complex 3D shapes that depend on several serial folds, as it resulted in misalignment between joining vertices [19].

The error in open-loop folding limits the precision and complexity of self-folded machines. One solution is to include angle sensors and use feedback control during folding. While many angle sensors exist, most are discrete, 3D components which are not compatible with the printable process. Resistive strain gauges printed using carbon-infused ink have been demonstrated with pneumatic self-folding hinges [21]. However, these sensors tended to drift over time, and each hinge had to be calibrated individually.

In this paper we describe a method for sensing and controlling fold angles using low-profile and printable sensors and actuators, and demonstrate their use in the development of a self-folding robot collective (Fig. 1). We describe the design and fabrication process of the SMC and introduce optical sensors and temperature sensors as a basis for feedback control. We characterize the embedded sensors and formulate a thermodynamic model to inform the control strategy. We then present a control strategy for angle control and assess its performance using experimental results. Finally we demonstrate an application of feedback-controlled self-folding of SMCs through the fabrication and operation of a small collective of autonomous self-folding robots.

## II. Design and Fabrication

### A. Actuator

In order to create self-folding hinges, we use SMCs activated by joule heating to enable electrical control of the folding process. We use pre-stretched polystyrene (PSPS), a type of SMP that is mechanically programmed to contract bi-directionally when heated above $100^\circ$C. Joule heating is achieved by supplying a current of $2.5$ A through a serpentine-patterned copper circuit that straddles the hinge, which heats the SMP above it. The SMP contracts above the hinge and forces the structure to fold in a pre-defined direction dictated by cuts in the supporting paper structure. The SMP thus provides a cheap, low profile and monolithic actuator that can be easily embedded as a layer in a composite material.

### B. Structure

The SMC consists of six layers, each laser-cut and bonded together using 125 $\mu$m silicone tape and cyanoacrylate (CA) glue (Fig. 2). Outer layers of paper serve as structural support while polyimide layers house circuitry and act as flexural hinges. Rectangular windows are cut in layers (C) and (D) to accommodate inwards-facing electrical components on layers (B) and (E). Once assembled, a final cut gives the composite its desired shape. To control actuation via Joule heating, a MOSFET in layer (B) is placed in parallel with a serpentine-patterned resistive circuit that straddles the hinge. A signal

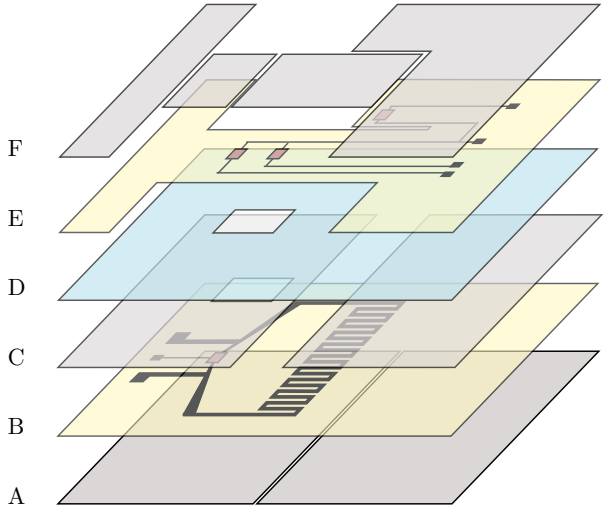


Fig. 2: The composite consists of six layers. (A) A 500 $\mu$m paper substrate, scored along the hinge at the center. (B) 12 $\mu$m thick copper traces forming resistive circuits etched onto a 18 $\mu$m thick polyimide sheet. (C) A layer of paper offsets the PSPS from the heating circuit. (D) A 500 $\mu$m thick PSPS contracts on thermal activation. (E) A second copper-polyimide flexible circuit houses sensors and control circuitry. (F) A paper substrate provides support for the sensor layer and bridges the hinge.

based on sensor readings regulates the voltage at the gate to either short current through the MOSFET or pass it through the resistive circuit. When the PSPS in (D) contracts, it pulls the two halves of (A) together and bends the polyimide layer (B) along the hinge. A paper substrate in (F) provides support for the sensor layer and bridges the hinge, bending at three locations as the structure folds.

### C. Angle Sensor

A phototransistor and infrared light-emitting diode (LED) pair provides a low cost, small and low profile means of measuring linear and angular displacements. Placed on either side of a hinge, the poses of both the LED and phototransistor change as the hinge folds, causing a measurable voltage drop across the phototransistor. A paper layer (F) in Fig. 2 is used as a rigid substrate for the flexible copper-polyimide printed circuit board (PCB) in layer (E). This constrains the LED and phototransistor to follow a pre-defined trajectory, where the voltage drop across the phototransistor as a result of its changing pose relative the LED has been calibrated to the hinge angle. A thermistor situated above the hinge remains stationary during the fold and is used to measure the rising temperature of the resistive circuit.

As discrete components, the sensor elements can be embedded in the surface of a structure using pick-and-place assembly prior to folding. However, direct contact with sunlight caused the phototransistors to saturate, limiting their use to indoors. Moreover, variations in ambient light indoors

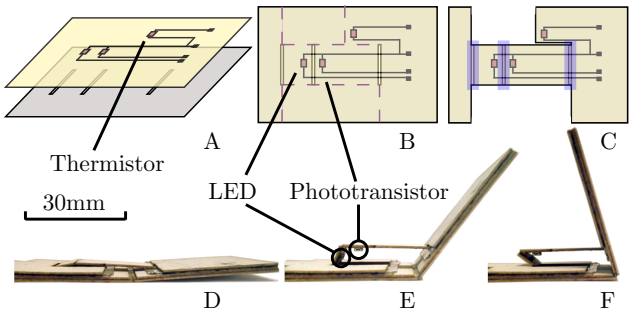


Fig. 3: By bonding and laser-cutting the layers in different stages, the sensors pop up away from the heated hinge as the structure folds. (A) The sensor layer is bonded to a paper substrate. (B) Dashed lines are laser-cut to release a four-bar linkage mechanism. (C) A finished sub-laminate; the three hinges of the four-bar linkage are highlighted in purple. The central hinge divides the phototransistor and LED, while the thermistor sits on the stationary substrate. (D), (E), (F) The structure during a fold.

were found to bias the readings by up to 15%. To mitigate interference from ambient light as well as adjacent LEDs, the sensor pair is inverted using a four-bar linkage (Fig. 3). This mechanism also causes the sensor pair to pop-up away from the hinge as the structure folds, preventing the sensor from being damaged or biased from the heat.

### *D. A Robot Collective*

In order to demonstrate closed-loop self-folding of SMCs, we designed and built a robot collective that is manufactured in one continuous laminate (Fig. 4). Initially joined by one monolithic sheet of SMP, individual robots in the collective are able to autonomously detach from one another, self-fold into pre-programmed configurations and navigate via phototaxis. Each robot is comprised of four equilateral triangles- a central body triangle, with each of its sides connecting to a triangular leg (Fig. 1). Each individual robot thus also takes the shape of an equilateral triangle, allowing tessellation within the collective.

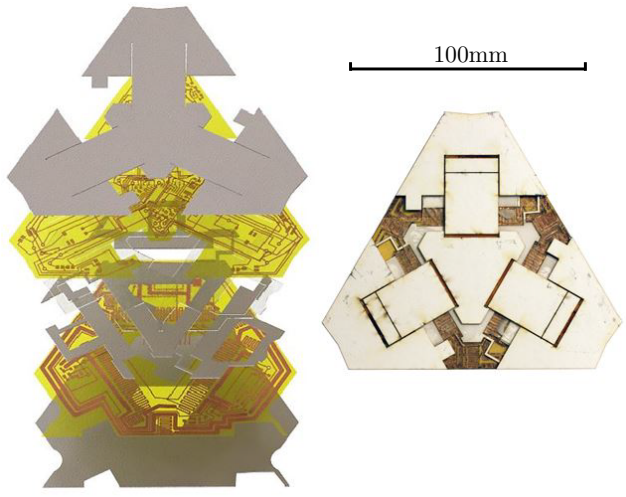


Fig. 4: (Left) Exploded CAD view of the layers comprising one self-folding robot unit. (Right) Photograph of an assembled robot in its unfolded configuration as viewed from below.

A single sheet of SMP connects individual robots in a collective during manufacturing, and a dedicated resistive circuit skirts these connections. By limiting the width of the SMP connections, individual robots are programmed to detach from one another by joule-heating the adjacent circuit; as the narrow SMP is unable to cause a fold, it pulls itself apart instead (Fig. 5), breaking the connection. Once this detachment is complete, each of the individual robots' three legs employs feedback control to fold to 90°, standing the robot up in the process. Enabling this using the limited torque produced by the SMP required several design iterations and motivated the robots' triangular shape, maximising the hinge length and thus the torque-mass ratio. Lastly, a fifth resistive circuit detaches a small module that connected each robot to an external current source used for joule heating, leaving each untethered robot to navigate freely using a small on-board battery. Each robot expends approximately 30 W for two minutes on joule-heating to enable detachment and self-folding, while locomotion draws under 200 mW. The detachment module uses the same circuitry used for folding a hinge via joule-heating. It is bonded to four copper pads on the robot using a hot melt adhesive, electrically connecting the robot to the external 2.5A current source as well as connecting the gate of the module's MOSFET to the robot's on-board controller.

Following detachment and self-folding, we use vibration motors to actuate the collective while minimizing the need for kinematic complexity. The legs remain stationary, and instead these motors enable locomotion via stick-slip motion, imposing the same non-holonomic constraints seen in differential drives. These motors have previously been used by the Kilobot, a collective of 1024 robots [22] containing just $14 worth of parts [23]. While mechanically simple and inexpensive, each robot is capable of both turning and walking straight, making it a useful testbed for collective behavior. Manufacturing irregularities between motors combined with the robots' small mass necessitate manually calibrating each motor to a unique PWM operating frequency in order to achieve the desired motion. This calibration occurs on a pre-folded robot prior to being mounted on the unfolded SMC, and feedback control ensures each robot's legs folds to the same angles as those on the pre-folded robot.

Two double-sided flexible PCBs provide circuitry and flexural hinges to join the central body to the legs. The upper PCB houses a controller, two batteries, two vibration motors for locomotion via stick-slip motion, five phototransistors to sense the legs' fold angles and to enable phototaxis, three thermistors to measure temperature at the hinges, a button and a three-color LED. The bottom PCB has four resistive circuits and attachment pads for a self-detaching module connecting the robot to an external supply. The PCBs are

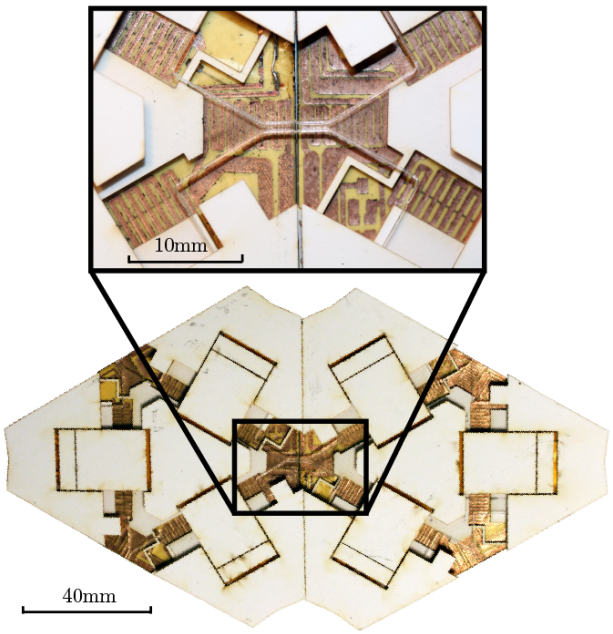


Fig. 5: Two connected robots in their unfolded configuration, as viewed from below. Serpentine-patterned resistive circuits at the vertices of the body triangles heat the SMP connecting the robots in the collective. The contractile force produced by the narrow bridge of SMP upon activation is not sufficient to create a hinge about which adjacent robots might fold, so the connection is pulled apart instead.

electrically connected to allow the controller to use sensors on the upper PCB to regulate current to the resistive circuits on the lower PCB.

## III. Sensor Characterisation

### A. Optical Sensor

To characterize a sensor pair, they are embedded in the four-bar linkage and swept through $0°$ to $120°$ in $1°$ increments, taking 30 measurements per increment. The experiments are carried out in a laboratory where fluorescent lamps with little infrared emissions provide the ambient light. The voltage across the phototransistor is recorded using a 10-bit analog-to-digital converter. This procedure is carried out five times and the mean $\pm 1$ standard deviation for each trial is shown in Fig. 6.

Once characterized, a given sensor pair has a repeatable output, showing an average standard deviation in error of $0.2°$. However, characterizing each sensor *in situ* each time a structure is rebuilt would be time-consuming, so we combine the characterizations of ten different sensor pairs to produce a general calibration curve (Fig. 7). The same measurement procedure was used as for Fig. 6, and the four-bar linkage was re-designed to increase resolution at smaller angles.

For a general characterization, we observe an average standard deviation in error of $3°$. The increase in error by an order of magnitude can be attributed to the manufacturing techniques used, where resolution is compromised for speed

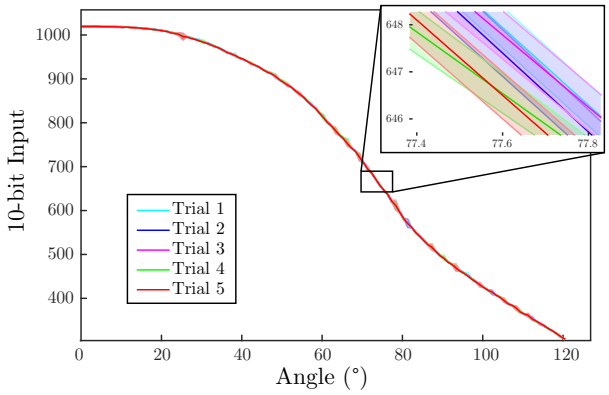


Fig. 6: Characterization curve for one LED-phototransistor pair. Output is shown for five sweeps, plotting mean $\pm 1$ standard deviation, $N = 30$.

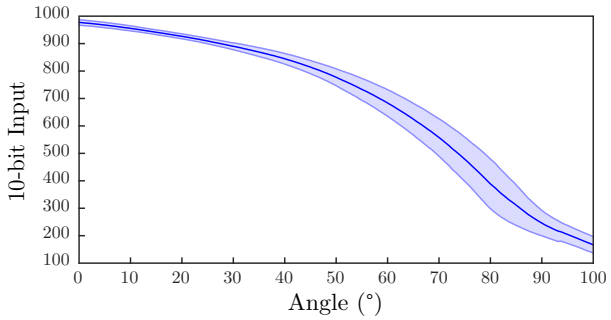


Fig. 7: General characterization curve combined from 10 individual LED-phototransistor pairs, plotting mean $\pm 1$ standard deviation, $N = 30$.

and ease of fabrication. The LED and phototransistor are manually aligned and hand-soldered, and in the course of folding undergo a linear separation of 0.5 mm to 5 mm so that a $3°$ error can be caused by misalignment of the components of just 120 $\mu$m. However, a procedure to automate accurate placement of the sensors could be incorporated at larger production scales to mitigate this issue.

### B. Temperature Sensor

To observe the relationship between output (fold angle) and input (current), current was applied to a resistive circuit in the structure described in Fig. 2 until folding began, at which point current was removed until folding stopped once more. The angle was measured using the optical sensor in the four-bar linkage and temperature was measured by a thermistor embedded in the SMC. Fig. 8(a) shows how temperature and angle evolve over time, while Fig. 8(b) shows the same data with temperature plotted against angle.

We refer to the temperature at which we observe a rapid increase in fold angle as the activation temperature ($T_a$). The $T_a$ required to further activate the material rises as the SMP contracts and fold angle increases. This is highlighted in Fig. 8(b) where four activation temperatures mark the start of increases in fold angle. It is also of note that the fold angle

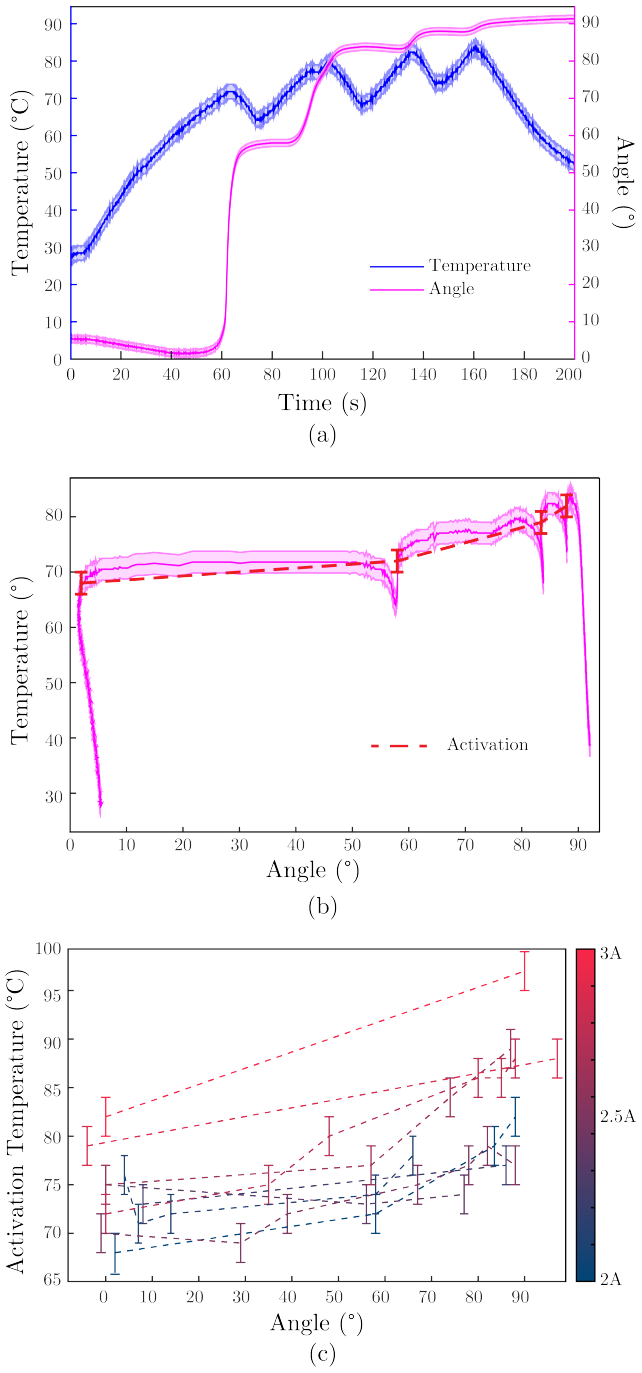


Fig. 8: **(a)** Change in fold angle and temperature over time as current is controlled manually. Current is set to 2.5A until folding begins, then set to 0A until folding stops, and repeated. **(b)** The same data as in Fig. 8(a), but plotting fold angle directly against temperature. Activation temperatures are joined by a dotted line and marked with error bars indicating $\pm 1$ standard deviation, $N = 30$. **(c)** Activation temperatures are recorded for nine sample hinges. Temperatures at which activation occurs are marked by error bars, and successive temperatures for individual hinges are joined by dotted lines.

in Fig. 8(b) decreases before reaching the first $T_a$; this is due to thermal expansion first lengthening the SMP.

Subsequent experiments show that the activation temperature varies significantly across test samples. Fig. 8(c) plots activation temperatures against fold angle for nine sample hinges. Dotted lines trace the successive activation temperatures for each individual hinge, as shown in Fig. 8(b). A reliable mapping of temperature to angle is thus not available and the rapid initial angular acceleration cannot easily be anticipated and mitigated ahead of time.

## IV. Modeling and Control

### A. Thermal Model

While temperature cannot be used to infer angle directly, we observe from Fig. 8(c) that $T_a$ is a monotonically increasing function of the fold angle. Since fold angle is monotonically increasing in time, it follows that $T_a$ is monotonically increasing in time as described in (1).

$$T_a[k] \geqslant T_a[k-1] \quad \forall k \tag{1}$$

This implies that higher temperatures are required to trigger folding at higher angles and later times, providing a heuristic lower bound to the temperature required to prevent folding at any time. Another observation is that higher activation temperatures occur when larger currents are used to heat the SMP. This is because larger currents lead to a quicker rise in temperature of the resistive circuit and a larger temperature gradient through the composite; as a significant percentage of the SMP's core volume must rise above $T_a$ in order to start folding, this temperature increase lags behind the measured temperature at the sensor.

To leverage the existence of a lower bound on $T_a$, we model the thermodynamics at the hinge in order to determine the time taken to return to $T_a$ from a given temperature. Equation (2) describes the continuous-time dynamics of the system given by a 1D lumped parameter model, modelling heat transfer as vertical conduction and convection through horizontal plates where $h$ is the heat transfer coefficient of the SMP, $A$ is the surface area of the SMP in contact with ambient air, $m$ is the mass of the SMP, $c$ is the specific heat capacity of the SMP, $k$ is the thermal conductivity of the SMP, $t_{smp}$ is the thickness of the SMP sheet, $T_{smp}$ is the temperature of the SMP bordering the resistive circuit, $T_o$ is the ambient air temperature and $Q$ is the heat flux generated by the resistive circuit. $Q$ is given by $Q = I^2R$

TABLE I: Thermal Model Parameters

| Variable | Symbol | Value | Unit |
|---|---|---|---|
| Transfer Coeff. | $h$ | 30.8 | W/m$^2$K |
| Surface Area | $A$ | 864 | mm$^2$ |
| Mass | $m$ | 237 | mg |
| Spec. Heat Capacity | $c$ | 1500 | J/kgK |
| Conductivity | $k$ | 0.2 | W/mK |
| Thickness | $t_{smp}$ | 0.5 | mm |
| Ambient Temperature | $T_o$ | 25 | °C |

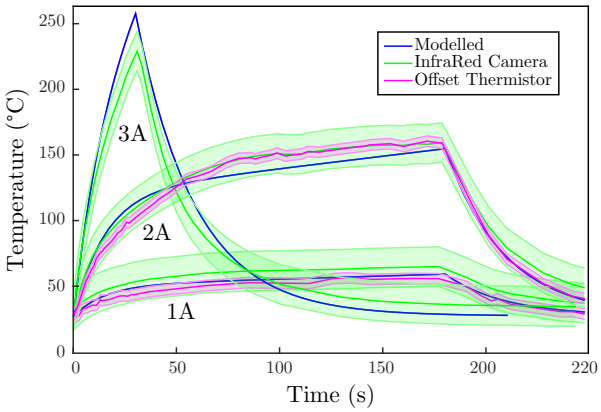


Fig. 9: Temperature of the resistive circuit as a result of Joule heating by 1A, 2A and 3A as predicted by the model and recorded by an infrared camera and thermistor.

where $I$ is the current and where $R$ is the resistance of the resistive circuit, where $R$ is modelled as a linear function of temperature. Fixed parameters are given in Table I.

$$\frac{dT_{smp}}{dt} = -\frac{hA}{mc}\left(\frac{k}{k+ht_{smp}}\right)T_{smp}(t) + \frac{1}{mc}Q_{gen}(t) - \frac{hA}{mc}T_o\left(\frac{ht_{smp}}{k+ht_{smp}} - 1\right) \quad (2)$$

Fig. 9 compares the modelled temperature as 1A, 2A and 3A are passed through the resistive circuit compared to data gathered by an infrared camera and a thermistor placed at the hinge. Thermistor data was not collected for 3A since the thermistor used was rated to a maximum of 150°C.

### B. Control Strategy

The SMP is a one-way actuator as it undergoes an irreversible shape change, so the control strategy is conservatively over-damped as an overshoot of the setpoint cannot be undone. We formulate a minimum time problem and employ bang-bang current control between 0A and 2.5A to regulate hinge temperature via Joule heating. Note that while the fold angle is an unknown function of hinge temperature, the commanded current input corresponds not to a fixed temperature, but to heat dissipated by the resistive circuit, i.e., a rate of change of temperature.

We compare the current temperature measurement ($T[k]$) to the last activation temperature ($T_a[k]$) and use (3) to calculate the time taken ($\Delta t[k]$) to decay back to $T_a[k]$, where $\dot{T}[k]$ is $\frac{dT_{SMP}}{dt}$ from (2) calculated at time $k$.

$$\Delta t[k] = \frac{1}{\dot{T}[k]}(T_a[k] - T[k]) \quad (3)$$

The control algorithm uses the angular derivative $\dot{\theta}[k]$ to estimate whether the current trajectory will overshoot the setpoint ($\theta^\star$) within $\Delta t[k]$ and then sets the binary input ($U[k]$) to either heat (1) or not heat (0) the SMP as shown in (4). This input is received by the gate of a MOSFET in parallel with the resistive circuit that will either short current through itself, thereby bypassing the resistive circuit, or force all the current through the resistive circuit, heating the SMP above.

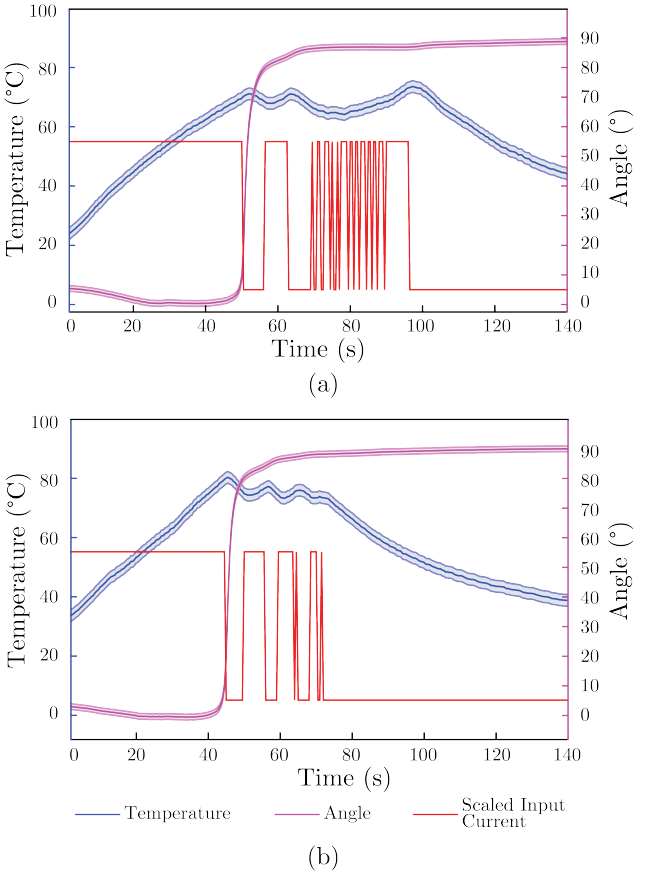


Fig. 10: **(a)** Step response to an angle setpoint of 90° using a model-free controller. **(b)** Step response to an angle setpoint of 90° using a model-based controller. The scaled input current reflects the value of the digital input signal U[k] varying between 0 and 1.

$$U[k] = \begin{cases} 0 & \text{if } \theta^\star < \theta[k] + \dot{\theta}[k]\Delta t[k] \\ 1 & \text{if } \theta^\star \geqslant \theta[k] + \dot{\theta}[k]\Delta t[k] \end{cases} \quad (4)$$

## V. Experimental Results

### A. Control of Fold Angle

Temperature and angle measurements are sampled at 60 Hz and low-pass filtered using a 30-sample averaging filter. A first order derivative of the angle is approximated by finite differences and the control algorithm runs at 2 Hz.

Fig. 10(a) shows a step response of the system to an angle setpoint of 90° using a black box derivative controller, excluding information about temperature. Fig. 10(b) shows the same step response using the model-based control strategy. The scaled input current reflects the value of the digital input signal $U[k]$ varying between 0 and 1, which corresponds to 0 A and 2.5 A passing through the resistive circuit, respectively.

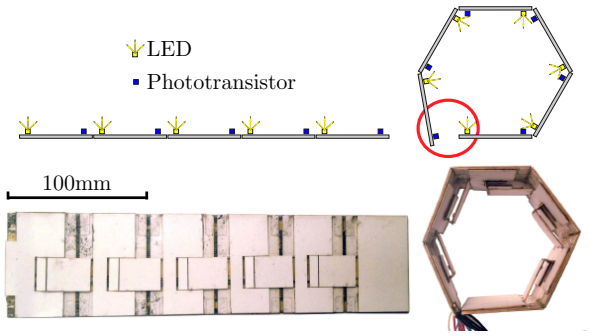


Fig. 11: (Top) A Hexagon in its unfolded (Left) and self-folded (Right) configurations, showing LEDs in yellow and phototransistors in blue. (Bottom) Photographs of the physical prototype.

The heuristic lower bound of activation temperature used by the model-based controller means that in order to stop folding, it does not need to drop below the last known activation temperature. This reduces the folding time by 20 seconds, where folding time is defined as the time between the first and last time the control signal $U[k]$ is set to 0. Given a setpoint $\alpha$, both control strategies result in a steady-state error of $0^\circ$ with a standard deviation of $1^\circ$ for five samples, on a truncated normal distribution on the interval $(\alpha, \infty)$.

Fig. 11 shows a self-folding hexagon fabricated by daisy-chaining five SMC hinges, folded in the ground plane to minimize opposing moments due to gravity. Initial experiments experienced several failure modes that were prevented over a number design iterations. These modes included delamination of the SMP from the adjacent paper layer, CA glue entering the hinge and solidifying during the bonding stage, too large structural masses to allow folding and melting of the SMP. However, once the manufacturing process and design was optimized, hinges showed a 100% success rate for 24 samples tested.

### B. A Robot Collective

A microcontroller on each robot is flashed with the same program consisting of four consecutive routines (Fig. 12). For simplicity, we initiate the first routine by pressing a button on each robot simultaneously; the robots then iterate autonomously through each routine. The first routine detaches each robot from its neighbours by heating the SMP connecting them open-loop for 80 seconds. The second routine folds the three legs to $90^\circ$ using the model-based control algorithm described above and stands the robots up in the process. In its unfolded configuration, the laminate is 4 mm thick, and after self-folding each robot stands at a height of 40 mm, resulting in a ten-fold increase in height. Once the optical sensors register that all legs have folded, the third routine signals the detachable module to heat itself open-loop for 30 seconds, detaching it by melting the hot melt adhesive bonding it to the robot. The fourth routine initiates locomotion via phototaxis (see supplemental video). Phototaxis was chosen as a simple method of simulating a navigation task for the folded robots, while leveraging the techniques developed for utilizing phototransistors during folding. This is achieved by programming robots to mimic the behaviour of Braitenberg vehicles by navigating in the direction of greatest light intensity. This is done by only actuating the motor on whichever leg holds the phototransistor measuring the least amount of light, thereby turning towards the light. When the two sensor measurements balance, both motors are actuated simultaneously in order to move forward (Fig. 13).

Forward locomotion occurs at 10 mm/s (0.2 body-lengths/s) and turning at $40^\circ$/s. This untethered locomotion is restricted to smooth horizontal surfaces and lasts for 200 seconds before depleting the batteries. Robot deployment yielded a success rate of 16/18. In both cases, failure was due to undiscovered open circuits leading to hinges not folding. These are likely a result of hand-soldering each individual robot's 75 components and 44 vias, as well as manual over-etching of the copper traces. An automated manufacturing process could therefore increase the success rate dramatically, making it viable for large scale deployment.

## VI. DISCUSSION

In this paper we demonstrate the increased fidelity of feedback-control over open-loop self-folding in SMCs. However, further studies are required to evaluate its performance over a full range of angles and in the presence of disturbances. We develop a thermal model of the temperature of the polymer during joule-heating via resistive circuits, and combine this with angle measurements from optical sensors embedded in the composite to formulate a control strategy. We achieve precise control of fold angles, however the angular velocity at $T_a$ often exceeds $30^\circ$/s, exacerbating the problem of overshoot for shallow angle setpoints. To mitigate this, smaller minimum fold angles could be achieved by bonding the SMP further out on either side of the hinge, also increasing torque at a cost to total angular range. More complex 3D geometries may need to rely on carefully planned folding order, and the failure of one hinge may result in the failure of the whole structure. As a form of proprioception, our angle sensors may lead to an accumulation of estimation errors for end-effector pose in long chains of serial folds. In the future, such error accumulation could be mitigated using e.g. *a posteriori* updates in a Kalman Filter.

Leveraging our results and the layered manufacturing process used in building SMCs, we present a robot collective that is fabricated in a single sheet; following transport in its flat, unfolded configuration, the individual robots in the collective are able to autonomously detach from one other, self-fold into pre-programmed configurations and navigate by phototaxis. This method allows the quick and inexpensive manufacturing of large numbers of robots that can be compactly transported before self-folding to begin their tasks. Well-suited applications that could be imagined include space robotics, where minimizing transport volume is critical, and search-and-rescue scenarios, where sheets of unfolded robot collectives could pass through cluttered entrances before deploying and beginning operations.


Fig. 12: (Left) A collective of four robots is fabricated as a single composite held together by one monolithic sheet of SMP. (Middle) Individual robots autonomously detach from one other by joule-heating the SMP connecting them, then self-fold their legs, standing up in the process. (Right) Self-folded robots use vibration motors and embedded phototransistors to navigate by phototaxis.

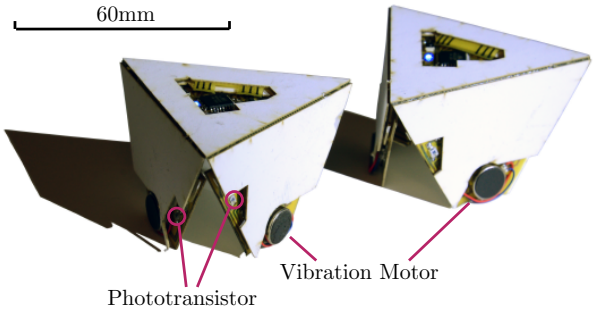


Fig. 13: Individual robots have two outwards-facing optical sensors on different legs that are angled at 120° from each other in order to determine the direction of greatest light intensity. A light source is placed out of frame to the right.

## REFERENCES


[1] A. M. Hoover, E. Steltz, and R. S. Fearing, "Roach: An autonomous 2.4 g crawling hexapod robot," in *Intelligent Robots and Systems, 2008. IROS 2008. IEEE/RSJ International Conference on*. IEEE, 2008, pp. 26–33.

[2] J. L. Silverberg, A. A. Evans, L. McLeod, R. C. Hayward, T. Hull, C. D. Santangelo, and I. Cohen, "Using origami design principles to fold reprogrammable mechanical metamaterials," *science*, vol. 345, no. 6197, pp. 647–650, 2014.

[3] K. Miura and U. K. K. (Japan), *Method of Packaging and Deployment of Large Membranes in Space*, ser. Institute of Space and Astronautical Science report. Institute of Space and Astronautical Sciences, 1985. [Online]. Available: https://books.google.de/books?id=nEoEHAAACAAJ

[4] E. D. Demaine, M. L. Demaine, and J. S. Mitchell, "Folding flat silhouettes and wrapping polyhedral packages: New results in computational origami," in *Proceedings of the fifteenth annual symposium on Computational geometry*. ACM, 1999, pp. 105–114.

[5] T. Tachi, "Origamizing polyhedral surfaces," *Visualization and Computer Graphics, IEEE Transactions on*, vol. 16, no. 2, pp. 298–311, 2010.

[6] J.-H. Na, A. A. Evans, J. Bae, M. C. Chiappelli, C. D. Santangelo, R. J. Lang, T. C. Hull, and R. C. Hayward, "Programming reversibly self-folding origami with micropatterned photo-crosslinkable polymer trilayers," *Advanced Materials*, vol. 27, no. 1, pp. 79–85, 2015.

[7] G. M. Whitesides and B. Grzybowski, "Self-assembly at all scales," *Science*, vol. 295, no. 5564, pp. 2418–2421, 2002.

[8] S. Felton, M. Tolley, E. Demaine, D. Rus, and R. Wood, "A method for building self-folding machines," *Science*, vol. 345, no. 6197, pp. 644–646, 2014.

[9] T. Halbert, P. Moghadas, R. Malak, and D. Hartl, "Control of a shape memory alloy based self-folding sheet," in *ASME 2014 International Design Engineering Technical Conferences and Computers and Information in Engineering Conference*. American Society of Mechanical Engineers, 2014, pp. V05BT08A041–V05BT08A041.

[10] A. Firouzeh and J. Paik, "Robogami: A fully integrated low-profile robotic origami," *Journal of Mechanisms and Robotics*, vol. 7, no. 2, p. 021009, 2015.

[11] Z. Zhakypov, M. Falahi, M. Shah, and J. Paik, "The design and control of the multi-modal locomotion origami robot, tribot," in *Intelligent Robots and Systems (IROS), 2015 IEEE/RSJ International Conference on*. IEEE, 2015, pp. 4349–4355.

[12] R. Niiyama, D. Rus, and S. Kim, "Pouch motors: Printable/inflatable soft actuators for robotics," in *Robotics and Automation (ICRA), 2014 IEEE International Conference on*. IEEE, 2014, pp. 6332–6337.

[13] L. Ionov, "Soft microorigami: self-folding polymer films," *Soft Matter*, vol. 7, no. 15, pp. 6786–6791, 2011.

[14] Y. Liu, R. Mailen, Y. Zhu, M. D. Dickey, and J. Genzer, "Simple geometric model to describe self-folding of polymer sheets," *Physical Review E*, vol. 89, no. 4, p. 042601, 2014.

[15] Y. Liu, J. K. Boyles, J. Genzer, and M. D. Dickey, "Self-folding of polymer sheets using local light absorption," *Soft Matter*, vol. 8, no. 6, pp. 1764–1769, 2012.

[16] S. M. Felton, M. T. Tolley, C. D. Onal, D. Rus, and R. J. Wood, "Robot self-assembly by folding: A printed inchworm robot," in *Robotics and Automation (ICRA), 2013 IEEE International Conference on*. IEEE, 2013, pp. 277–282.

[17] M. T. Tolley, S. M. Felton, S. Miyashita, L. Xu, B. Shin, M. Zhou, D. Rus, and R. J. Wood, "Self-folding shape memory laminates for automated fabrication," in *Intelligent Robots and Systems (IROS), 2013 IEEE/RSJ International Conference on*. IEEE, 2013, pp. 4931–4936.

[18] S. Miyashita, C. D. Onal, and D. Rus, "Self-pop-up cylindrical structure by global heating," in *Intelligent Robots and Systems (IROS), 2013 IEEE/RSJ International Conference on*. IEEE, 2013, pp. 4065–4071.

[19] M. T. Tolley, S. M. Felton, S. Miyashita, D. Aukes, D. Rus, and R. J. Wood, "Self-folding origami: shape memory composites activated by uniform heating," *Smart Materials and Structures*, vol. 23, no. 9, p. 094006, 2014.

[20] B. Shin, S. M. Felton, M. T. Tolley, and R. J. Wood, "Self-assembling sensors for printable machines," in *Robotics and Automation (ICRA), 2014 IEEE International Conference on*. IEEE, 2014, pp. 4417–4422.

[21] X. Sun, S. M. Felton, R. J. Wood, and S. Kim, "Printing angle sensors for foldable robots," in *Intelligent Robots and Systems (IROS), 2015 IEEE/RSJ International Conference on*. IEEE, 2015, pp. 1725–1731.

[22] M. Rubenstein, A. Cornejo, and R. Nagpal, "Programmable self-assembly in a thousand-robot swarm," *Science*, vol. 345, no. 6198, pp. 795–799, 2014.

[23] M. Rubenstein, C. Ahler, and R. Nagpal, "Kilobot: A low cost scalable robot system for collective behaviors," in *Robotics and Automation (ICRA), 2012 IEEE International Conference on*. IEEE, 2012, pp. 3293–3298.